Effects of Particle Shape and Size on Black Liquor and Biomass Reactivity

Hong Lu, Justin Scott, Kelly Echols, Paul Foster, Bryan Ripa, Russell Farr, Larry L. Baxter
Chemical Engineering Department
Brigham Yong University
350 CB
Provo, UT 84602

ABSTRACT

Experimental and theoretical investigations indicate how particle shape and size influence biomass combustion rates. Experimental samples include flake-like, cylinder-like, and equant (nearly spherical) shapes with similar particle masses and volumes but different surface areas. These samples passed through a laboratory reactor in a nitrogen atmosphere and a maximum reactor wall temperature of 1600 K. A separately developed computer and image analysis system determined particle surface-area-to-volume ratios based on three orthogonal particle silhouettes. Experimental data indicate that equant particles react more slowly than the other shapes, with the difference becoming more significant as particle mass increases and reaching a factor of two for particles less than 1 mm in diameter.

A one-dimensional particle model simulates the rapid pyrolysis process of particles with different shapes. The model characterizes particles in three basic shapes (sphere, cylinder, and flat plate). With the particle geometric information (particle aspect ratio, volume, and surface area) included, this model can be modified to simulate the devolatilization process of biomass particles of any shape. Model simulations of the three shapes agree nearly within experimental uncertainty with the data. Model predictions extended to a wider range of sizes predict the effects of shape and size on yields and overall mass conversion rates. The near-spherical particle losses mass most slowly and its conversion time significantly differs from those of flake-like particles and cylinder-like particle when particle equivalent diameter increases. Little difference exists between the cylinder- and plate-like particles. Low-ash fuels yield up to 95% volatiles during high-temperature pyrolysis. Both particle shape and size affect the product yield distribution. Near-spherical particles exhibit lower volatile and higher tar yields relative to aspherical particles with the same mass. Volatile yields decrease with increasing particle size for particles of all shapes.

INTRODUCTION

At least two compelling forces drive global interest in renewable energy supplies: (1) increasing concern about environmental impacts associated with fossil fuels and nuclear energy; and (2) increasing anxiety regarding the security and longevity of fossil fuel resources. One potential strategy that addresses both concerns is the supplementing traditional, dominantly fossil fuels with renewable biomass fuels, since biomass fuels come from indigenous sources and can be essentially CO_2-neutral (considering the carbon cycle in atmosphere) if derived from sustainable cultivation practices. Thermal conversion (combustion and gasification) represents the most common commercial utilization of biomass. Black liquor and hog fuel used at pulp and paper mills represent by far the largest contributions to non-hydro renewable energy in the country. Both current and future technologies employed in the pulp and paper industry benefit from more accurate understanding of the processes occurring in the conversion systems. This investigation focuses on issues common to most conversion systems – particle combustion characteristics.

Black liquor and biomass particles commonly have more irregular shapes and much larger sizes than pulverized coal or other entrained-flow, low-grade fuels, with typical aspect ratios between 2 and 15. Larger particle sizes establish the potential for large internal temperature and composition gradients that complicate combustion models. At present, particle models used in computational fluid dynamics (CFD) codes and elsewhere generally assume spherical, isothermal biomass particles [1, 2]. Furthermore, various particle shapes result in different particle exterior surface-area-to-volume ratios, which are essential to heat and mass transfers and further affect the devolatilization and oxidation rates. Spheres represent an extreme case with lowest surface-area-to-volume ratios of any shape.

A substantial experimental and modeling literature for biomass particle pyrolysis processes exists, with varying kinetic mechanisms and related parameters. A one-step global model, which is described by one global reaction

suffices for relatively simple applications [3-7]. The drawback of the one-step model is that it cannot predict the variation of total mass or individual product yield distributions with temperature and heating conditions. Typical wood applications use one- or two-stage multiple reaction models [8-12]. Two-step models include a primary stage, during which wood thermally decomposes to produce light gases, tars, and chars, and a secondary stage, during which tars undergo additional cracking to produce gases. Much more sophisticated devolatilization models exist [13, 14], including some under development by this research group [15], and these will be incorporated into this analysis in the future, but the present simple models are adequate to illustrate the impacts of shape and size on particle conversion.

Intra-particle heat and mass transfer effects must be accounted for to accurately predict the devolatilization rate of mm-sized particles and consequently heat release in the boilers [16]. Biomass particle models usually include mass, energy, and momentum transport equations [17-30]. Few of these particle models simulate aspherical shapes but several are suitable for incorporation into CFD codes. The paucity of experimental data suitable for validating these model predictions compromises the potential contributions of such models to engineering or scientific investigations.

This investigation summarizes experimental devolatilization conversion rates for sawdust particles of three shapes in an entrained-flow reactor together with a model that predicts these data nearly within their experimental uncertainty. A particle model is developed to simulate the devolatilization of biomass particle of any shape. Effects of particle shape and size on devolatilization behaviors are investigated over a wider range of conditions than are available from experimental data to evaluate overall impacts of aspherical shapes in practical applications.

EXPERIMENTAL METHOD

Fuel Properties

The samples used in this study are sawdust particles with same volume and different shapes. Three shapes are considered: flake-like, cylinder-like, and near-spherical. The sawdust was first separated using sieves, then aerodynamically classified. Finally, different aspect ratios were separated by sieves again. The samples were put in an oven at 90 ^{o}C for two hours before feeding. To measure the particle surface area and volume, three images were taken from three orthogonal directions for the particle. The particle volume and surface area were calculated using a 3D shape reconstruction code, which is developed in the combustion lab at Brigham Young University. The particle volume was verified by measuring over 2000 particles with the particle density known as 650 kg/m^3. The samples are shown in Figure 1. Other data of the samples are tabulated in Table I.

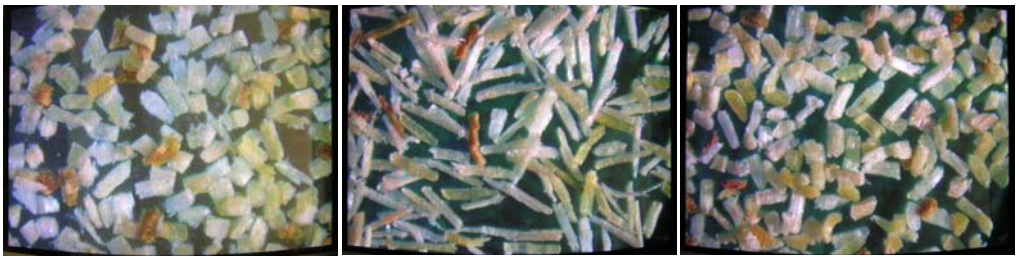

(a) flake-like particle (b) cylinder-like particle (c) near-spherical particle

Figure 1 Photographs of sawdust particles of different shape.

An entrained flow reactor is used in this study. As is shown in Figure 2, the reactor includes feeding section, reactor body, collection section, and separation section. The feeding section consists of a syringe feeder and a water-cooled feeding probe, which can obtain a feeding rate as low as 1.0 gm/hr. An electrically heated preheater can heat the secondary gas up to 500 ^{o}C before it enters the reactor. The reactor body is electrically heated using Kanthal super heating elements, providing a maximum wall temperature of 1650 K. The reactor also provides up to 0.5 seconds residence time, and the residence time can be changed by adjusting the relative distance between the feeding probe and collection probe. When particle reaches the collection probe at the bottom of the reactor, it will be quenched down by nitrogen gas. The flow rate ratio of the quench nitrogen and the secondary gas is about 7 ~ 10. Char will be collected in the first cyclone separator, which has a cutting point of 25 μm. The second cyclone separator has a cutting point of 5 μm, which is capable of collecting most of the condensed tar. Finally, the very fine particles are collected in the filter. The pore size of the filter is 1 μm.

Table I Sample properties

Sample	Flake-like	Cylinder-like	Equant
Volume ($\times 10^{-11}$ m^3)	1.697	1.682	1.794
Equivalent diameter (mm)	0.32	0.32	0.325
Surface area ($\times 10^{-7}$ m^2)	4.91	4.79	3.438
Aspect ratio	4.0 (width/thickness)	6.0	1.65

Experimental Setup and Procedure

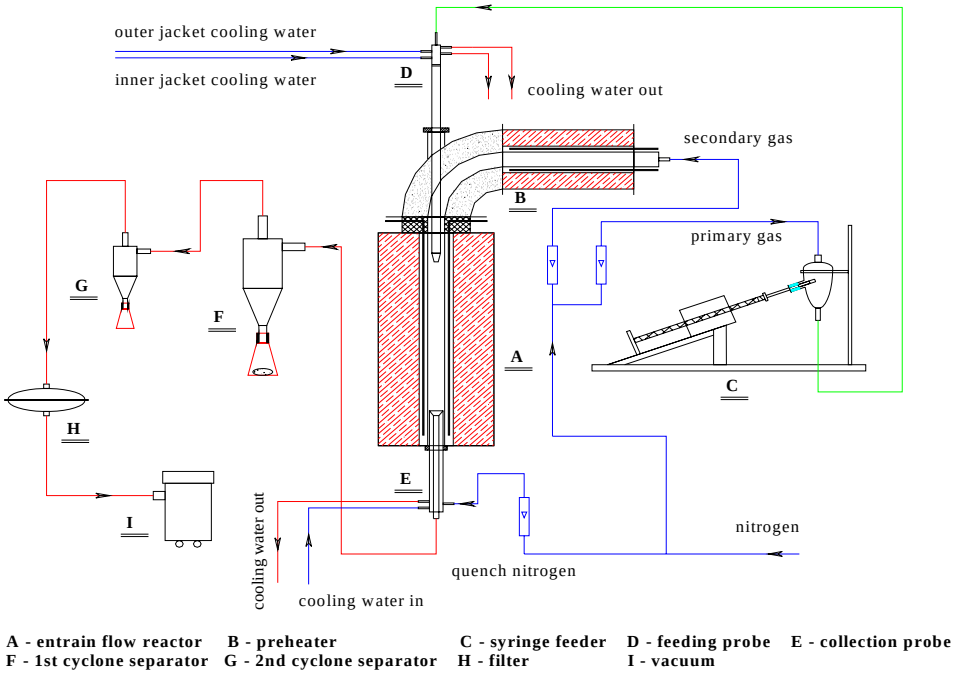

Figure 2 Entrained flow reactor schematic diagram.

With the sawdust samples prepared above, devolatilization experiments are conducted on this entrained flow reactor in nitrogen environment. Mass loss data as functions of residence time have been collected.

Description of the Mathematical Model

When the biomass particle is traveling through the entrained flow reactor, it is exposed to both radiation and convective heat transfer. This devolatilization process involves the heating of raw biomass or organic materials in the absence of oxidizer, the thermal degradation of the biomass components, mass transport of the devolatilization products in the particle by means of advection and diffusion, and blowing of the gas products at the surface of the particle. The two-stage wood pyrolysis kinetics model, shown in Figure 3, is chosen for this particle model since it is capable of predicting the product yields and distribution variations with temperature and heating rate which are significantly influenced by particle shape and size.

Moisture in wood is divided into two categories: free water and bound water [31]. Moisture content above the fiber saturation point (FSP) is considered as free water, and below as bound water. The average FSP is 30% according to [31], which is the weight of water in the wood as a percentage of the weight of ovendry wood. Free moisture vaporizes from the surface at a rate determined by the surface vapor pressure, the moisture in the bulk flow and the surface area of the particle. Bound water does not vaporize in a manner similar to free moisture.

Four basic methods, including a thermal model, describe wood drying under combustion heat fluxes [32]. A chemical reaction using an Arrhenius expression describes the release of this moisture, consistent with recommendations from the literature. Figure 4**Error! Reference source not found.** illustrates the drying scheme of moisture. The particles used in these experiments were dried prior to use to maximize the particle size that can react in our residence-time-limited reactor. Drying of this nature removes all of the free moisture and bound water.

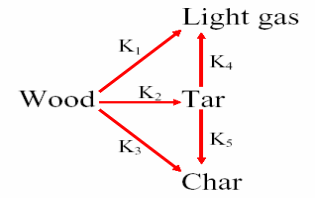

Figure 3 Reaction scheme for thermal decomposition of biomass

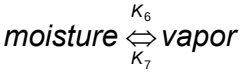

Figure 4 Drying scheme of moisture.

Assumptions included in the mathematical model described below include:

all properties are assumed to be transient and one dimensional;

local thermal equilibrium exists between the solid and gas phase in the particle, so temperatures and their gradients are the same for the solid and gas;

gases behave as ideal gases, including both relationships between pressure, temperature, and specific volume and dependence of heat capacity on temperature only;

particle aspect ratios and shapes do not change during devolatilization – a simplifying assumption for this case but not required by the model in general;

heat and mass transfer at particle boundaries increase relative to that of a sphere by the ratio of the particle surface to that of a volume-equivalent sphere.

In the particle model, the particle shapes are represented by a parameter n. A spherical particle is described by n = 2, cylinder particle n = 1, and flat plate particle n = 0. Before the biomass particle enters the reactor, it is assumed that it is filled by inert gas. So there are totally seven species are considered in the model: biomass, char, moisture, light gas, tar, water vapor, and inert gas. The mass conservation of each species, the momentum, and the total energy equations, as well as the initial and boundary conditions are illustrated in equations 1- 23.

The biomass temporal mass balance contains three consumption terms, one each for the reactions to light gas, tar, and char, where all terms in this expression and most terms in the following expressions are functions of both time and position.

$$\frac{\partial \rho_B}{\partial t} = -(K_1 + K_2 + K_3)\rho_B \qquad 1$$

Similarly, the char temporal mass balance contains two source terms, one from the conversion of biomass to char and one for the char yield from the secondary reactions of tar

$$\frac{\partial \rho_C}{\partial t} = K_3 \rho_B + \varepsilon K_5 \rho_T \qquad 2$$

The temporal moisture mass balance contains a loss associated with conversion to vapor and a source term associated with water vapor readsorption into the particle, the latter having an explicit dependence on gas velocity as suggested by the literature [32]

$$\frac{\partial \rho_M}{\partial t} = -K_6 \rho_M + \varepsilon K_7 \rho_g Y_V u \qquad 3$$

The conservation equations for all gas-phase components (light gas, water vapor, tar, and inert gas) include temporal and spatial gradients and source terms and can be written as follows

$$\frac{\partial}{\partial t}\varepsilon\rho_g Y_i + \frac{1}{r^n}\frac{\partial}{\partial r}(r^n \varepsilon \rho_g Y_i u) = \frac{1}{r^n}\frac{\partial}{\partial r}(r^n \varepsilon D_{eff,i}\rho_g \frac{\partial Y_i}{\partial r}) + S_i \qquad 4$$

where $i = T$ for tar, G for light gas, V for water vapor, and I for inert gas and source terms are defined as follows

$$S_T = K_2\rho_B - \varepsilon K_4 \rho_T - \varepsilon K_5 \rho_T \qquad S_G = K_1\rho_B + \varepsilon K_4 \rho_T$$
$$S_V = K_6\rho_M - K_7 \varepsilon \rho_g Y_V u \qquad S_I = 0 \qquad 5$$

The total gas-phase continuity equation is defined as the sum of these species and has the form

$$\frac{\partial}{\partial t}\varepsilon\rho_g + \frac{1}{r^n}\frac{\partial}{\partial r}(r^n \varepsilon \rho_g u) = S_g \qquad 6$$

where

$$S_g = K_1\rho_B + K_2\rho_B - \varepsilon K_5 \rho_T + K_6 \rho_M - \varepsilon K_7 \rho_g Y_V u \qquad 7$$

The gas-phase velocity in the particle obeys a Darcy-law-type expression

$$u = -\frac{\eta}{\mu}\frac{\partial P}{\partial r} \qquad 8$$

where

$$P = \frac{\rho_g R_g T}{M_W} \qquad 9$$

and M_W is the mean molecular weight and the permeability is expressed as a mass-weighted function of the individual solid-phase permeabilities

$$\eta = \frac{\rho_B}{\rho_{B,0}}\eta_B + \left(1 - \frac{\rho_B}{\rho_{B,0}}\right)\eta_C \qquad 10$$

Arrhenius expressions describe the temperature dependence of the kinetic rate coefficients for reactions 1-6 illustrated in Figure 3and **Error! Reference source not found.**

$$K_i = A_i \exp(-\frac{E_i}{RT}) \quad (11)$$

The energy conservation equation describes

$$\begin{aligned}
&\frac{\partial}{\partial t}\left[\left(\rho_B \hat{H}_B + \rho_C \hat{H}_C + \rho_M \hat{H}_M\right) + \varepsilon\rho_g\left(Y_G \hat{H}_G + Y_I \hat{H}_I + Y_T \hat{H}_T + Y_V \hat{H}_V\right)\right] \\
&+ \frac{1}{r^n}\frac{\partial}{\partial r}\left[r^n \varepsilon\rho_g u\left(Y_G \hat{H}_G + Y_T \hat{H}_T + Y_I \hat{H}_I + Y_V \hat{H}_V\right)\right] = \frac{1}{r^n}\frac{\partial}{\partial r}\left(r^n k_{eff}\frac{\partial T}{\partial r}\right) \\
&+ \frac{1}{r^n}\frac{\partial}{\partial r}\left[r^n \rho_g \varepsilon\left(\begin{array}{l} D_{eff,T}\frac{\partial Y_T}{\partial r}\hat{H}_T + D_{eff,G}\frac{\partial Y_G}{\partial r}\hat{H}_G + D_{eff,V}\frac{\partial Y_V}{\partial r}\hat{H}_V \\ + D_{eff,I}\frac{\partial Y_I}{\partial r}\hat{H}_I \end{array}\right)\right]
\end{aligned} \quad (12)$$

where

$$\hat{H}_i = \hat{H}^0_{i,f} + \int_{T_0}^{T} Cp_i dT \quad (13)$$

and subscript *i* represents each of the four gas-phase components as before.

This form of the energy equation relates to standard theoretical analyses [33] for multi-component systems. In Equation 12, the first term represents the energy accumulation; the second term represents energy convection; the third term (first term after the equals sign) accounts for conduction heat transfer, and the last term accounts for energy associated with diffusion of species in the gas phase,. The last term generally contributes only negligibly to the overall equations and is commonly justifiably ignored.

The effective particle thermal conductivity includes radiative and conductive components with some theoretical basis [34, 35] and with empirical verification for wood [26].

$$k_{eff} = k_{cond} + k_{rad} \quad (14)$$

where the particle structure is assumed to be close to the upper limit for thermal conductivity, that is, is assumed to have high connectivity in the direction of conduction,

$$k_{cond} = \varepsilon k_{gas} + (1-\varepsilon)\left[\frac{\rho_B}{\rho_{B,0}}k_B + \left(1-\frac{\rho_B}{\rho_{B,0}}\right)k_C\right] \quad (15)$$

and where radiation contributes approximately to the third power of the temperature

$$k_{cond} = \frac{\varepsilon\sigma T^3 d_{pore}}{\omega} \quad (16)$$

Initial conditions are assumed from experimental conditions for a non-reacting particle. That is, at $t = 0$,

$$
\begin{aligned}
&P(t=0,r)=P_{atm}\\
&T(t=0,r)=300\,K\,(typically)\\
&u(t=0,r)=0\\
&Y_l(t=0,r)=1\\
&Y_T(t=0,r)=Y_V(t=0,r)=Y_G(t=0,r)=0
\end{aligned}
\qquad 17
$$

Boundary conditions at the particle center are determined by symmetry, that is, at $r = 0$

$$
\begin{aligned}
&\left.\frac{\partial P}{\partial r}\right|_{t,r=0}=0\Rightarrow u(t,r=0)=0\\
&\left.\frac{\partial T}{\partial r}\right|_{t,r=0}=0\\
&\left.\frac{\partial Y_l}{\partial r}\right|_{t,r=0}=0
\end{aligned}
\qquad 18
$$

Boundary conditions at the particle outer surface are defined by external conditions of pressure, heat and mass flux, and

$$
\begin{aligned}
&P(t,r=r_p)=P_{atm},\\
&\left.\frac{\partial Y_i}{\partial r}\right|_{r=t,r_p}=0\\
&k_{eff}\left.\frac{\partial T}{\partial r}\right|_{r=t,r_p}=\theta_T h_f R_{SA}\left(T_f-T\right)+R_{SA}\omega\sigma\left(T_w{}^4-T^4\right)
\end{aligned}
\qquad 19
$$

where θ_T represents the blowing factor [33]. R_{SA} represents the exterior surface area ratio, which is the surface area of the particle divided by the characteristic surface area as follows

$$
\begin{aligned}
&R_{SA}=SA/(4\pi R_P{}^2)\\
&R_{SA}=SA/(4\pi R_P{}^2 AR)\\
&R_{SA}=SA/(4R_P{}^2 AR^2)
\end{aligned}
\qquad 20
$$

for spheres, cylinders, and flat plates, respectively

Each shape employs heat transfer coefficients developed for that particular shape. Correlations suitable for andom particle orientation during flight appear in the literature for some particles. Where such a model is not available the characteristic length of the particle is calculated using the average length of the particle. For near-spherical particle, Masliyah's prolate spheroid model [36] provides a suitable correlation, as indicated in Equation 21.

$$
Nu=1.05+0.6\,\mathrm{Re}^{0.65}\,\mathrm{Pr}^{0.33}
\qquad 21
$$

Cylinders at low Reynolds numbers adopt the correlation of Kurdyumov [37] (see Equation 22). Expression for W_0 and W_1 appear in detail in the literature [37].

$$Nu = W_0(\mathrm{Re})\mathrm{Pr}^{0.33} + W_1(\mathrm{Re}) \quad (22)$$

The heat transfer coefficient of flat plate is shown in Equation 23

$$Nu = 0.644\,\mathrm{Re}^{0.5}\,\mathrm{Pr}^{0.343} \quad (23)$$

The kinetic parameters for wood pyrolysis found in literatures vary over a wide range. They are usually measured at low to moderate temperature (usually < 900 K). No high-temperature kinetic data for the two-stage scheme have been reported. Font et al. [9] presented kinetic data for the three primary reactions that are found to be comparable to what Nunn et al. [3] reported for the single reaction kinetic data for hardwood in the high-temperature range (573 ~ 1373 K). Font et al.'s results are used in this model. The pre-exponential factors, activation energy, and heat of reactions of all the reactions used in this model appear in Table II.

Table II Kinetic parameters of wood pyrolysis process

Reaction no.	frequency factor (s^{-1})	activation energy (kJ/mol)	reference	Heat of reaction kJ/kg	reference
1	1.52×10^{7}	139.2	[9]	-418	[17]
2	5.85×10^{6}	119	[9]	-418	[17]
3	2.98×10^{3}	73.1	[9]	-418	[17]
4	4.28×10^{6}	107.5	[38]	42	[39]
5	1.0×10^{5}	107.5	[40]	42	[39]
6	5.13×10^{10}	88	[32]	-2,440	[32]
7	$T < 95$ ℃ $K_7 = 125\mathrm{cm}^{-1}$ $T > 95$ ℃ $K_7 = 0\mathrm{cm}^{-1}$		[32]	2,440	[32]

The physical properties of the biomass particles significantly affect the heat and mass transfer process [23, 41]. In this work, temperature-dependent heat capacity correlations are used for all species. The heat capacity of biomass and char adopt the model suggested by Merrick [42]. Gronli et al. [27] suggested a correlation for tar heat capacity, which is based on some typical pyrolysis tar components (closely related to benzene). All physical properties are listed in Table III.

Table III Physical properties of biomass particles

Variable	Value	Reference
Wood density ρ_B	650 kg/m^3	
Porosity ε	0.4	
Emissivity ω	0.75	
Permeability η	η_B = 0.01 Darcy	[27]
	η_C = 10 Darcy	[27]
Thermal conductivity k	k_{gas} = 0.026 W/m.K	[43]
	k_B = 0.11 W/m.K	[44]
	k_C = 0.071 W/m.K	[44]
Pore size d_{pore}	3.2×10^{-6} m	[26]
Molecular weight M	M_T = 145 kg/kmol	[26]
	M_G = 31 kg/kmol	[26]
	M_l = 28 kg/kmol	
	M_V = 18 kg/kmol	
Viscosity μ	$\mu_{gas} = 3\times10^{-5}$ Pa.s	[43]
Diffusivity D_{eff}	$D_{eff} = 1.0\times10^{-6}$ m^2/s for all	[17]
Heat capacity Cp (J/kg.K)	$Cp_B = \left(\frac{1000R_g}{7.72}\right)\left[g\left(\frac{380}{T}\right) + 2g\left(\frac{1800}{T}\right)\right]$	[42]
	$Cp_C = \left(\frac{1000R_g}{11.3}\right)\left[g\left(\frac{380}{T}\right) + 2g\left(\frac{1800}{T}\right)\right]$	[42]

Where, $g(x) = \frac{x^2 e^x}{(e^x - 1)^2}$

$Cp_T = -100+4.4\times T-0.00157\times T^2$ [27]

$Cp_G = 770+0.629\times T-0.000191\times T^2$ [27]

$Cp_l = 950+0.188\times T$ [27]

$Cp_M = 4180$

$Cp_V = 2220$

The mass conversion equations of biomass, char, and moister are solved using fourth-order Runge-Kutta method. Control volume (finite volume) [45] method is applied to solve the gas species mass conservation equations and energy conservation equations. A power-law scheme and the SIMPLE algorithm are used to accelerate the convergence of the solution procedure.

RESULTS AND DISCUSSIONS

The wall and gas temperatures measured by type B thermocouples during sawdust pyrolysis experiments appear in Figure 5. Based on these average temperature profiles of reactor and gas, the mathematical model simulates the devolatilization process of the sawdust particle with the specific shapes described in the sample preparation section. Figure 6 illustrates the mass loss history of the three samples. Both the experimental data and model predictions show that the near-spherical particle losses mass most slowly compared with the other two shapes, while the flake-like particle devolatilizes slightly faster than cylinder-like particle. For each of the three samples, the slope of the model prediction is found to be steeper than that of the experimental data. This can be explained by the fact that an imperfect size and/or shape distribution of the sample may exist, even though the samples are considered to be very uniform after the delicate sample preparation procedure. These variations in shape and size tend to smooth the observed curve of mass loss vs. time as the small particles react faster than the larger particles.

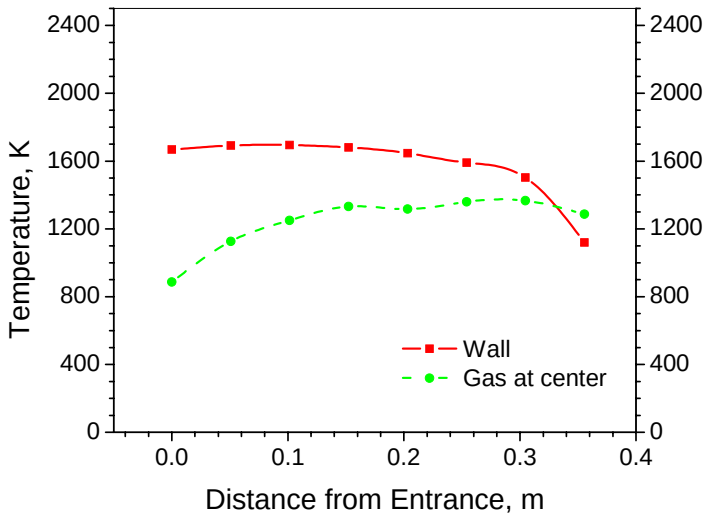

Figure 5 Reactor wall temperature and gas temperature at center

The data and the model agree quantitatively that near-spherical particles react more slowly than do less symmetrical particles. The mass losses differ by as much as a factor of two during most of the particle histories based on both the predictions and the measurements. These data indicate that at these relatively small sizes, asphericity plays a significant role in overall conversion.

The experimental data and model predictions also show that the near-spherical particles yield slightly lower volatiles relative to the other shapes. This is caused by a combination of different particle temperature histories due to the particle shape and longer average path lengths for tars to travel in spherical particles compared to the

aspherical counterparts. The flake-like and cylinder-like particles have larger surface area and smaller thickness, which result in a higher heating rate and faster heat and mass transfer to the particle. The predicted surface and center temperatures for the three samples are illustrated in Figure 7. As expected, the near-spherical particle heats up slower than the other two shapes.

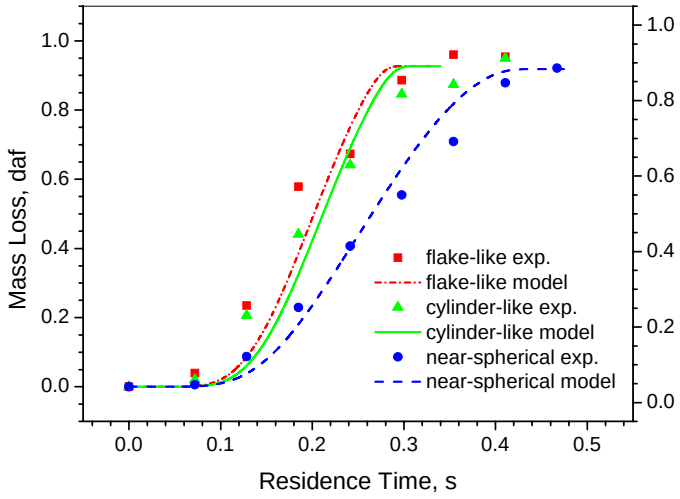

Figure 6 Mass loss histories of sawdust particles with different shapes

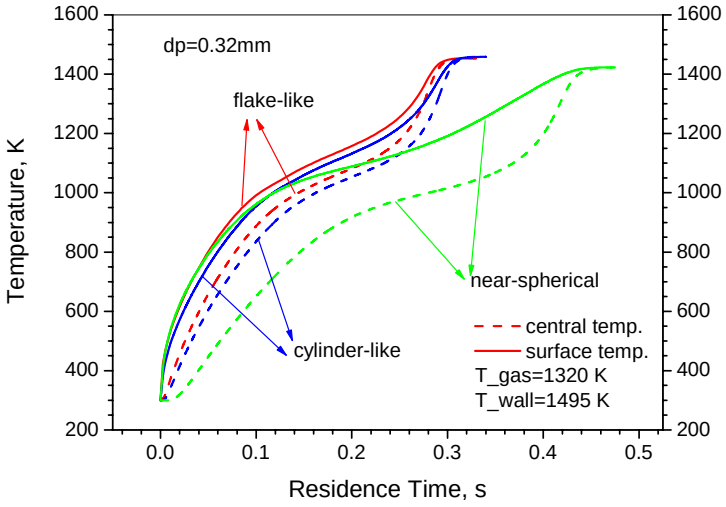

Figure 7 Particle temperature history comparison

The composition gradients inside the near-spherical particle are predicted using the model, as shown in Figure 8. Both the biomass density and the char density changes are illustrated at the particle center and surface boundary.

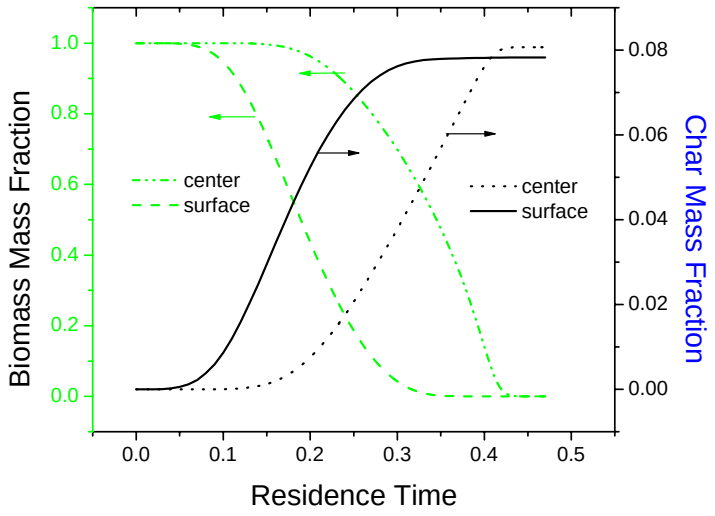

Figure 8 Composition of the near-spherical particle as functions of time

The particle size of the samples used in the experiment is limited by the reactor length since it can only provide a maximum residence time of about 0.5 seconds. However, the model developed and validated against the nominal 300 μm particle data can provide estimates for larger particle behavior. Assuming the same aspect ratios for all of the three particles with different shapes, the conversion times predicted as a function of equivalent diameter appear in Figure 9. Pyrolysis conversion time increases with increasing equivalent diameter as would be expected. Additionally, conversion time difference between spherical and aspherical particles increases with increasing particle size. In addition, the effects of particle shapes and sizes on volatile yields are investigated using the model. As shown in Figure 10, the volatile yield of near-spherical decreases with increasing particle size. Both flake-like and cylinder-like particles behavior similarly.

The effect of particle shape on conversion time and product distribution should be more apparent for large particles than small particles. Large particles that sustain substantial internal temperature and composition gradients transfer heat and mass at rates that scale with surface area. Spheres have the lowest surface area to volume ratio of all shapes and should therefore transfer heat and mass at slower rates than aspherical particles of the same volume/mass. By contrast, particles with little or no internal temperature and compositions gradients transfer mass and heat at rates proportional to total particle volume. These typically small particles are less sensitive to shape than are larger particles of the same material in the same environment. These data and the analyses quantify these theoretical trends and indicate that particles as small as 0.3 mm equivalent diameter experience significant differences in conversion rate. This renders spheres poor choices for many if not most biomass fuels. This concept is similar to but not identical with using a Biot number to determine when internal temperature (and composition) gradients are significant. The Biot number determines when internal temperature (and composition) gradients can be ignored ($Bi < 0.1$) but does not in itself help determine how to treat the impacts of shape on such gradients when they shouldn't be ignored.

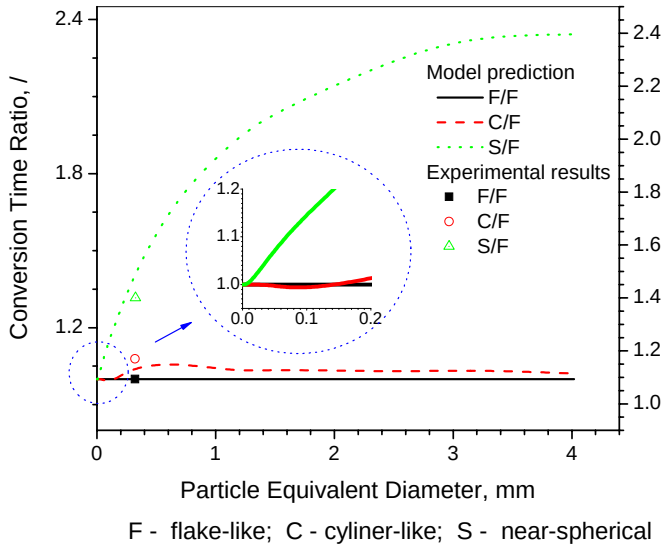

Figure 9 Conversion time vs. particle equivalent diameter

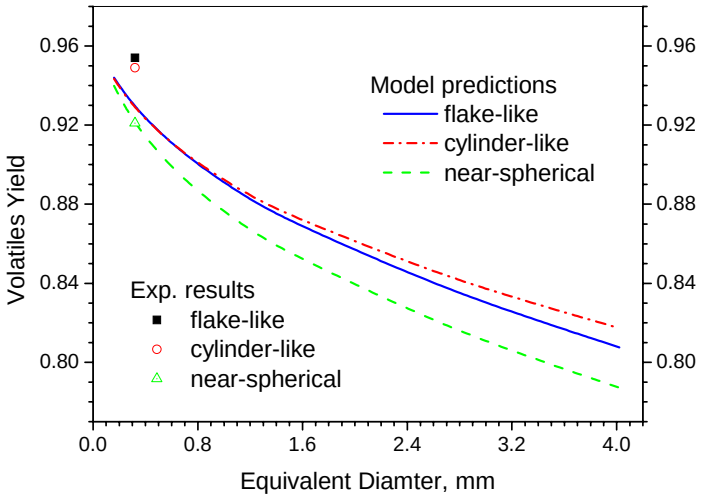

Figure 10 Volatile yields comparison of various particle shape and size

CONCLUSIONS

Both experimental and theoretical investigations indicate the impact particle shape and size have on overall particle reactivity. Experiments conducted on biomass particles at relevant temperatures and a variety of well-characterized shapes indicate that particle shape impacts overall reaction rates relative to those of spheres with the same mass/volume by factors of two or more at relatively small sizes. Theoretical models developed and validated against the data indicate that the impact of shape increases with increasing size and is much greater at sizes relevant to black liquor and biomass utilization in the pulp and paper industry. Generally speaking, spherical mathematical approximations for fuels that either originate in or form aspherical shapes during combustion poorly represent combustion behavior when particle size exceeds a few hundred microns. This includes a large fraction of the particles in both biomass and black liquor combustion.

NOMENCLATURE

A_i	pre-exponential factor, s^{-1}
AR	aspect ratio,
Cp	heat capacity, $J.kg^{-1}.K^{-1}$
d_{pore}	pore diameter, m
D_{eff}	effective diffusivity, $m^2.s^{-1}$
E_i	activation energy, $J.mol^{-1}$
h_f	heat transfer coefficient, $W.m^{-1}.K^{-1}$
$\hat{H}$	enthalpy, $J.kg^{-1}$
k	thermal conductivity, $W.m^{-1}.K^{-1}$
η	permeability, m^2
K_i	rate constant, s^{-1}
M	molecular weight, $kg.kmol^{-1}$
M_W	gas average molecular weight, $kg.kmol^{-1}$
n	shape factor
Nu	Nusselt number,
P	pressure, Pa
Pr	Prandtl number
r	radius coordinate, m
Re	Reynolds number
R_g	universal gas constant, $J.mol^{-1}.K^{-1}$
Rp	particle radius, m
R_{SA}	surface area ratio,
t	time, s
SA	surface area
S_i	source term
T	temperature, K
u	gas velocity, $m.s^{-1}$
Y	mass fraction,
Greek symbols	
ε	porosity,
μ	viscosity, Pa.s
ρ	density, $kg.m^{-3}$
σ	Boltzman constant, $W.m^{-2}.K^{-4}$
ω	emissivity,
$-\Delta H$	heat of reaction, $J.kg^{-1}$
Subscript	
0	initial value or reference state
B	biomass
1, …, 7	reaction
C	char
con	conductivity
g	gas phase
G	light gas
I	inert gas
M	moisture
rad	radiation
V	water vapor
T	tar
w	wall

ACKNOWLEDGEMENTS

This investigation is supported by US Department of Energy (DOE) / EE Office of Industrial Technologies. Thanks are given to Dr. Thomas Fletcher for help in model development. Mark Vickers developed the particle shape reconstruction code and Paul Foster, Kelly Echoes, Brian Spears, and Russ Johnson contributed to this project.

REFERENCES

1. O'Dowd, W., et al., *Moisture and char reactivity modeling in pulverized coal combustors.* Combustion Science and Technology, 2001. **172**(1): p. 35-69.

2. Fletcher, D.F., et al., *CFD based combustion model of an entrained flow biomass gasifier.* Applied Mathematical Modelling, 2000. **24**(3): p. 165-182.

3. Nunn, T.R., et al., *Product compositions and kinetics in the rapid pyrolysis of sweet gum hardwood.* Industrial & Engineering Chemistry, Process Design and Development, 1985. **24**(3): p. 836-844.

4. Varhegyi, G., et al., *Kinetics of the thermal decomposition of cellulose, hemicellulose, and sugar cane bagasse.* Energy & Fuels, 1989. **3**(3): p. 329-335.

5. Antal, M.J.J. and V. Gabor, *Cellulose Pyrolysis Kinetics: the Current State of Knowledge.* Ind. Eng. Chem. Res., 1995. **34**: p. 703-717.

6. Antal, M.J.J., G. Varhegyi, and E. Jakab, *Cellulose pyrolysis kinetics: Revisited.* Industrial & Engineering Chemistry Research, 1998. **37**(4): p. 1267-1275.

7. Guo, J. and A.C. Lua, *Kinetic study on pyrolysis of extracted oil palm fiber. Isothermal and non-isothermal conditions.* Journal of Thermal Analysis and Calorimetry, 1st Brazilian

Congress on Thermal Analysis and Calorimetry (I CBRATEC), Mar 29-Apr 2 1998, 2000. **59**(3): p. 763-774.

8. Di Blasi, C., *Comparison of semi-global mechanisms for primary pyrolysis of lignocellulosic fuels.* Journal of Analytical and Applied Pyrolysis, 1998. **47**(1): p. 43-64.

9. Font, R., et al., *Kinetics of the pyrolysis of almond shells and almond shells impregnated with CoCl₂ in a fluidized bed reactor and in a Pyroprobe 100.* Industrial & Engineering Chemistry Research, 1990. **29**(9): p. 1846-1855.

10. Thurner, F. and U. Mann, *Kinetic investigation of wood pyrolysis.* 1981. **20**(3): p. 482-488.

11. Brown, A.L., D.C. Dayton, and J.W. Daily, *A study of cellulose pyrolysis chemistry and global kinetics at high heating rates.* Energy and Fuels, 2001. **15**(5): p. 1286-1294.

12. Babu, B.V. and A.S. Chaurasia, *Modeling, simulation and estimation of optimum parameters in pyrolysis of biomass.* Energy Conversion and Management, 2003. **44**(13): p. 2135-58.

13. Niksa, S., A.R. Kerstein, and T.H. Fletcher, *Predicting Devolatilization at Typical Coal Combustion Conditions with the Distributed-Energy Chain Model.* Combustion and Flame, 1987. **69**(2): p. 221-228.

14. Solomon, P.R., T.H. Fletcher, and R.J. Pugmire, *Progress in Coal Pyrolysis.* Fuel, 1993. **72**(5): p. 587-597.

15. Pond, H.R., T.H. Fletcher, and L. Baxter. *Prediction of Tar and Light Gas During Pyrolysis of Black Liquor and Biomass*. in *3rd Annual Joint Meeting of the U.S. Sections of the Combustion Institute*. 2003. Chicago, IL.

16. Bharadwaj, A., L.L. Baxter, and A.L. Robinson, *Intra-Particle Effects in Biomass Devolatilization: Experimental Results and Model Predications.* Submitted for publication, 2004.

17. Chan, W.-C.R., M. Kelbon, and B.B. Krieger, *Modelling and experimental verification of physical and chemical processes during pyrolysis of a large biomass particle.* Fuel, 1985. **64**(11): p. 1505-1513.

18. Shen, M.S., et al., *Kinetic Studies of Rapid Oil Shale Pyrolysis. 2. Rapid pyrolysis of Oil Shales in a Laminar-flow Entrained Reactor.* Fuel, 1991. **70**(11): p. 1277-1284.

19. Di Blasi, C., *Numerical simulation of cellulose pyrolysis.* Biomass and Bioenergy, 1994. **7**(1-6): p. 87-98.

20. Di Blasi, C., *Kinetic and heat transfer control in the slow and flash pyrolysis of solids.* Industrial & Engineering Chemistry Research, 1996. **35**(1): p. 37-46.

21. Di Blasi, C., *Heat, momentum and mass transport through a shrinking biomass particle exposed to thermal radiation.* Chemical Engineering Science, 1996. **51**(7): p. 1121-1132.

22. Miller, R.S. and J. Bellan, *A Generalized Biomass Pyrolysis Model Based on Superimposed Cellulose, Hemicellulose and Lignin Kinetics.* Combustion Science and Technology, 1997. **126**: p. 97-137.

23. Di Blasi, C., *Influences of Physical Properties on Biomass Devolatilization Characteristics.* Fuel, 1997. **76**: p. 957-964.

24. Liliedahl, T. and K. Sjostrom, *Heat transfer controlled pyrolysis kinetics of a biomass slab, rod or sphere.* Biomass and Bioenergy, 1998. **15**(6): p. 503-509.

25. Jalan, R.K. and V.K. Srivastava, *Studies on Pyrolysis of a Single Biomass Cylindrical Pellet Kinetic and Heat Transfer Effects.* Energy Conversion & Management, 1999. **40**: p. 467-494.

26. Janse, A.M.C., R.W.J. Westerhout, and W. Prins, *Modelling of Flash Pyrolysis of a Single Wood Particle.* Chemical Engineering and Processing, 2000. **39**: p. 239-252.

27. Gronli, M.G. and M.C. Melaaen, *Mathematical model for wood pyrolysis - comparison of experimental measurements with model predictions.* Energy and Fuels, 2000. **14**(4): p. 791-800.

28. Brown, A.L., et al., *Design and Characterization of an Entrained Flow Reactor for the Study of Biomass Pyrolysis Chemistry at High Heating Rates.* Energy and Fuels, 2001. **15**(5): p. 1276-1285.

29. Hagge, M.J. and K.M. Bryden, *Modeling the impact of shrinkage on the pyrolysis of dry biomass.* Chemical Engineering Science, 2002. **57**(14): p. 2811-2823.

30. De Diego, L.F., et al., *Modeling of the devolatilization of nonspherical wet pine wood particles in fluidized beds.* Industrial and Engineering Chemistry Research, 2002. **41**(15): p. 3642-3650.

31. Forest Products Laboratory United States Department of Agriculture Forest Service, *Chapter 3, Physical Properties and Moisture Relations of Wood*, in *Wood Handbook: Wood as an Engineering Material*. 1999, Forest Products Society: Madison, Wisconsin. p. 3-5.

32. Bryden, K.M. and M.J. Hagge, *Modeling the combined impact of moisture and char shrinkage on the pyrolysis of a biomass particle.* Fuel, 2003. **82**(13): p. 1633-1644.

33. Bird, R.B., W.E. Stewart, and L.E. N., *Transport Phenomena*. Second ed. 2002, New York / Chichester / Weinheim / Brisbane / Singapore / Toronto: John Wiley & Sons, Inc.

34. Robinson, A.L., S.G. Buckley, and L.L. Baxter, *Thermal Conductivity of Ash Deposits 1: Measurement Technique.* Energy & Fuels, 2001. **15**: p. 66-74.

35. Robinson, A.L., et al., *Thermal Conductivity of Ash Deposits 2: Effects of Sintering.* Energy & Fuels, 2001. **15**: p. 75-84.

36. Masliyah, J.H. and N. Epstein, *Numerical solution heat and mass transfer from spheroids in steady axisymmetric flow.* Prog. Heat Mass Transfer, 1972. **6**: p. 613-632.

37. Kurdyumov, V.N. and E. Fernandez, *Heat transfer from a circular cylinder at low Reynolds numbers.* Journal of Heat Transfer, Transactions ASME, 1998. **120**(1): p. 72-75.

38. Liden, C.K., F. Berruti, and D.S. Scott, *A kinetic model for the production of liquids from the flash pyrolysis of biomass.* Chemical Engineering Communications, 1988. **65**: p. 207-221.

39. Koufopanos, C.A., et al., *Modelling of the Pyrolysis of Biomass Particles. Studies on Kinetics, Thermal and Heat Transfer Effects,.* The Canadian Journal of Chemical Engineering, 1991. **69**: p. 907-915.

40. Di Blasi, C., *Analysis of convection and secondary reaction effects within porous solid fuels undergoing pyrolysis.* Combustion Science and Technology, 1993. **90**: p. 315-340.

41. Raveendran, K., A. Ganesh, and K.C. Khilart, *Influence of Mineral Matter on Biomass Pyrolysis Characteristics.* Fuel, 1995. **74**(12): p. 1812-1822.

42. Merrick, D., *Mathematical models of the thermal decomposition of coal. 2. Specific heats and heats of reaction.* Fuel, 1983. **62**(May): p. 540-545.

43. Kansa, E., J., H.E. Perlee, and R.F. Chaiken, *Mathematical model of wood pyrolysis including internal forced convection.* 1977. **29**(3): p. 311-324.

44. Lee, C.K., R.F. Chaiken, and J.M. Singer, *Charring pyrolysis of wood in fires by laser simulation.* Symp (Int) on Combust, 16th, MIT, Aug 15-20 1976, 1976: p. 1459-1470.

45. Patankar, S.V., *Numerical Heat Transfer and Fluid Flow*. Series in computational methods in mechanics and thermal sciences, ed. W.J.M.a.E.M. Sparrow. 1980: Taylor & Francis.